Available online at www.sciencedirect.com

SciVerse ScienceDirect

Ceramics International 39 (2013) 6041–6050

CERAMICS INTERNATIONAL

www.elsevier.com/locate/ceramint

Fabrication and characterization of ceramic coatings with alumina–silica sol-incorporated α-alumina powder coated on woven quartz fiber fabrics

Hao-Ran Lu, Chang-An Wang*

Department of Materials Science and Engineering, State Key Laboratory of New Ceramics and Fine Processing, Tsinghua University, Beijing 100084, China

Received 17 December 2012; received in revised form 8 January 2013; accepted 8 January 2013
Available online 17 January 2013

Abstract

The formation and properties of dense silica/α-alumina coatings derived from alumina–silica sol-incorporated coarse alumina powder (median particle size $d_{50}=0.509$ μm) using $Al(NO_3)_3 \cdot 9H_2O$ and tetraethyl orthosilicate as precursors have been investigated. Phase compositions and thermal evolution analysis of the coatings as well as interface microstructure between the coatings and the matrix were characterized by means of XRD, XRF, DSC-TG, TEM, SEM supplemented with EDS, and tensile strength tester. Silica/α-alumina coatings combined with quartz fiber matrix are homogeneously integrated with distinct inter-diffusion near the interface. The heat conduction mechanism of the quartz fiber matrix was influenced by the dense silica/α-alumina ceramic coatings, and the prepared coatings provide practical thermodynamic stability and desired mechanical strength for the woven quartz fiber fabrics.

Keywords: Quartz glass fibers; SiO_2/Al_2O_3 coatings; Sol–gel technique

1. Introduction

Quartz glass fibers have many unique properties at high temperature, such as high thermal shock resistance, low coefficient of thermal expansion and excellent mechanical properties. Therefore, they are extensively used as materials for wave-transparent, thermal insulation and load-bearing parts in aerocrafts [1–7]. However, a severe limitation of quartz glass fibers is their susceptibility to crystallization when exposed to high-temperature environments, especially above 1423 K, which usually leads to serious fiber brittleness and degradation, and hence becomes an urgent barrier to the use of quartz glass fiber as heat insulation and shielding function materials in high-temperature oxidizing systems [8,9]. Applying coatings on quartz glass fibers is considered an effective way to prevent devitrifying under such conditions.

In our previous research, Zr–Zn based glaze coating and high temperature-resistant inorganic phosphate plastic coating were applied on the surface of the quartz glass fibers. But, owing to the mismatch of thermal expansion coefficient and the interfacial crack between matrix and coating, both of the coatings cannot be successfully coated on the quartz glass fibers matrix surface. Sol–gel chemistry offers a simple and convenient pathway for the synthesis of advanced materials and surface coatings. The sol–gel chemistry can provide efficient incorporation of organic components into the inorganic structures in solution under extraordinarily mild thermal conditions. Therefore ceramic coatings prepared by sol–gel processing are widely used as coatings and corrosion resistant films on structural components. Sol–gel coatings also offer a potentially cost-effective way of protecting quartz glass fibers from crystallizing at high temperatures. However, an important limitation of this process is that the thickness of the coatings is limited to less than 1 μm because of the stresses induced by drying and densification processes of the gel, leading to the cracking of the film, In order to obtain much thicker crack-free films, the classical sol–gel method can be modified by incorporating ceramic powders into sols [10–12].

By means of the modified process, it is very easy to form a slurry, which can be coated onto the substrate of interest,

*Corresponding author. Tel.: +86 010 627 854 88.
E-mail addresses: wangca888@126.com, wangca@tsinghua.edu.cn (C.-A. Wang).

0272-8842/$ - see front matter
http://dx.doi.org/10.1016/j.ceramint.2013.01.020

by mixing a ceramic powder with a sol, and the process has been successfully applied to a variety of ceramic materials [13–15] (e.g., piezoelectric ceramics and porous ceramic matrix). Recently, there are a few reports on the preparation of Al_2O_3–SiO_2 composite sol–gel coatings on quartz glass fibers. Relatively thick (>10 μm) Al_2O_3–SiO_2 composite coatings have been fabricated using this modified processing for chemically bonding the alumina sol and silica sol. These coatings are typically deposited from a water-based composite sol by dip-coating technology and cured at relatively low temperatures, typically 350–450 °C. In the present work, the modified technique is a simple extension whereby Al_2O_3 powder (~0.5 μm) is incorporated into the Al_2O_3–SiO_2 sol, creating a stable suspended slurry. This suspension is then deposited on the quartz glass fiber substrate, and the crystallization behavior of quartz glass fibers, the phase constitution and thermal behavior of coatings, interface microstructure between coatings and matrix, tensile strength and anti-crystallization ability were investigated.

2. Experimental procedure

2.1. Preparation of sol

The silica sol was prepared by mixing tetraethylorthosilicate ($Si(OEt)_4$; TEOS; 99.9%) with ethanol and HNO_3 (1.6 M) as catalysts. TEOS was then hydrolyzed and the resulting silica sol was magnetically stirred for 2 h. In order to catalyze hydrolysis and condensation reactions, the pH value of the silica sol was adjusted to a value close to 2 by adding hydrogen nitrate (HNO_3, 1.6 M). Nitric acid contributes in long Si–O–Si chain formation and therefore promotes coating formation. $Al(NO_3)_3 \cdot 9H_2O$ was then dissolved by distilled water and was magnetically stirred for 2 h at 45 °C. The molar ratio of tetraethylorthosilicate to aluminum nitrate in the prepared sol was maintained at 1:3 according to the stoichiometric mullite.

2.2. Sample preparation

Prior to coating deposition, the fibers were sintered at 450 °C for 4 h and then degreased ultrasonically in ethanol for 10 min and in distilled water in an ultrasonic bath for 10 min, and were finally dried at 120 °C for 30 min in an infrared ray drying oven. Commercial calcined α-alumina powders (~0.5 μm) were added to the silica/alumina sol, the amount of mixed powder dispersed in the silica/alumina sol represented 25 wt% of the total mixture. Low pH prevents fast gelation of the sol, thus giving enough time for Al_2O_3 powder dispersion. In order to obtain excellent and stable suspension, the pH of slurry was again adjusted, and then the suspension was stirred for 3 h to achieve homogeneous and stabilized dispersion. The surface of the quartz glass fibers pretreated in above way was coated with SiO_2/Al_2O_3 slurry layers by the dip-coating method with a constant withdrawal velocity of 12 mm min^{-1}. In order to remove the solvents from the gel, the samples were first dried at 120 °C for 30 min in the infrared ray drying oven. After drying, the densification processing was performed by a heat treatment at 400 °C for 30 min (the silicon molybdenum rods electric furnace heating rate: 2 °C/min). In this way, one-, two-, three-, and four-layered SiO_2–Al_2O_3 coatings were obtained. Fig. 1 illustrates the technique processing of modified sol–gel dip-coating.

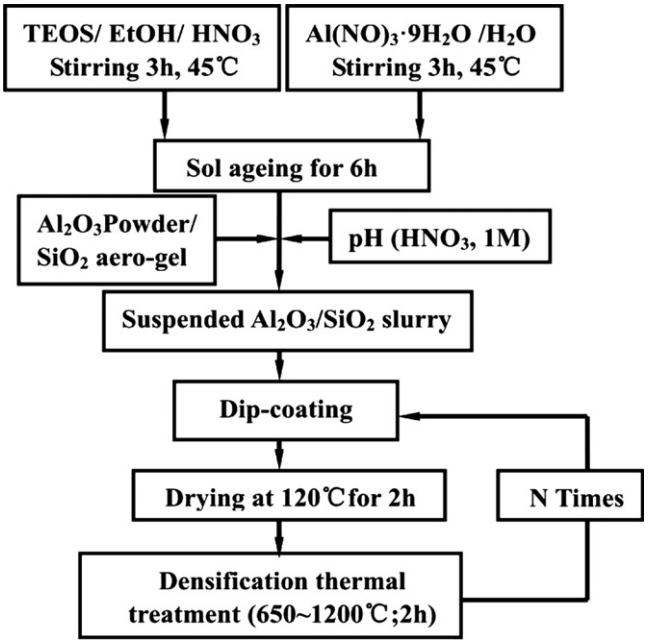

Fig. 1. Modified sol–gel dip-coating technique processing.

2.3. Characterization

The particle size distribution of commercial α-Al_2O_3 powder was examined on a Mastersizer-2000 laser particle analyzer. The viscosity of the alumina–silica sol and of the sol-incorporated α-Al_2O_3 slurry were measured by a MCR300 senior expand rheometer. The chemical analyses of quartz fibers were performed by an XRF-1800 model X-ray fluorescence spectrometer (Shimadzu, Tokyo, Japan). The thermal evolution analysis of the sol-coated alumina powder was examined on the TG/DTA 7300 model thermal analyzer (Seiko, Japan) by heating to 1445 °C at 10° C/min using α-Al_2O_3 powder as standard reference. The phase compositions of coatings were identified by a Bruker-D8 Advance Da Vinci X-ray diffractometer with CuKα radiation (40 mA, 40 kV), in the range of 2θ from 10° to 90°. The microstructure and element distribution of the prepared coatings were imaged by a JSM-7001F field emission scanning electron microscope supplemented with energy diffraction spectrum (SEM-EDS, JEOL Japan). The diffraction pattern and micro-morphology of sintered quartz fibers coated with alumina–silica coatings were characterized by a JEM-2100F field emission transmission electron microscope (TEM, JEOL, Japan). The tensile strength of

the quartz fibers before and after coating were performed with an Instron 1343 tensile-torsional low-frequency fatigue machine (Fig. 2).

2.4. Thermal-conductivity measurements

Thermal diffusivity of the samples was measured by means of the laser flash technique(LFA 427, Netzsch GmbH) for slab samples (Φ12.7 mm × d1.5 mm) in air atmosphere. Before thermal-diffusivity measurements, both the front and the back faces of each specimen were coated with a thin layer of carbon which was done to prevent direct transmission of the laser beam through the translucent specimens and be beneficial to the full absorption and emission of energy. Appropriate corrections were made in the thermal diffusivity calculations to account for the presence of these layers. Thermal conductivity [16] of the sample was obtained using the followed equation:

$$\lambda = \alpha \rho c_p \quad (1)$$

where α is thermal diffusivity, ρ represents bulk density of the free-standing coating measured by Archimedes' Method, and c_p is the specific heat measured by Differential Scanning Calorimetry. The accuracy of the calculated thermal conductivities is limited to the uncertainties of the factors related to the Eq. (1). In this study, the specific heat was measured via a differentiated scanning calorimeter instrument (Pegasus 404C-DSC, Netzsch) which encloses a systematic standard deviation of $\pm 4\%$ according to the manufacturer. Moreover, the bulk density represents the average value of three morphologically identical coatings. Ultimately, the thermal diffusivities used in the calculations are based on an average of three measured values for each temperature condition.

3. Results and discussion

3.1. Thermal damage of quartz fibers

According to the listed results by the analysis of X-ray fluorescence spectra (Table 1), the relative concentration of SiO_2 and Al_2O_3 in raw quartz glass fibers are determined as 98.29 and 1.01 wt%, respectively. The thermal evolution curves of the quartz fibers are plotted in Fig. 3, with the temperature range up to 1445 °C at 10 °C/min using α-Al_2O_3 powder as standard reference. As seen, the mass loss maximum of 4.5% in the range 40–900 °C is attributed to the dissociation of organic additive from the surface of the samples. In addition, it is suggested that the broader exothermic bands at 985–1435 °C in the DSC curve without any weight variation shown in the TG curve should be ascribed to the crystallization of α-cristobalite from quartz glass fibers. The composition of quartz glass fibers is mainly uncrystallized quartz, and owing to the wider transitional temperature region and the slower transitional rate, there is no distinctly exothermic peak of phase transformation. Fig. 4 shows the XRD patterns of quartz glass fibers before and after different heat treatments. It can be seen that the fiber is almost amorphous before heat treatment. It is found that the onset crystallization temperature of α-cristobalite is near 1100 °C, and the peak intensity of the α-cristobalite phase became stronger with

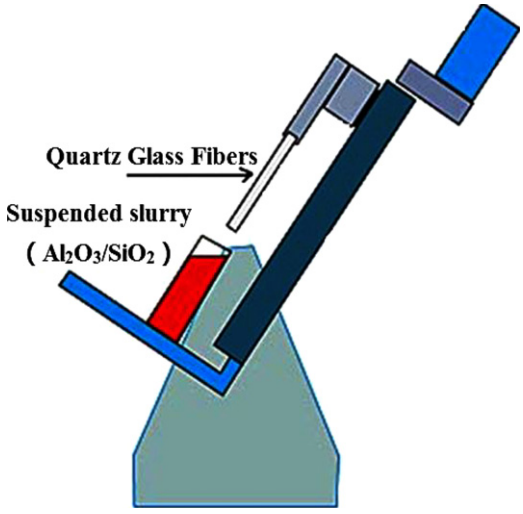

Fig. 2. Schematic diagram of dip-coating machine.

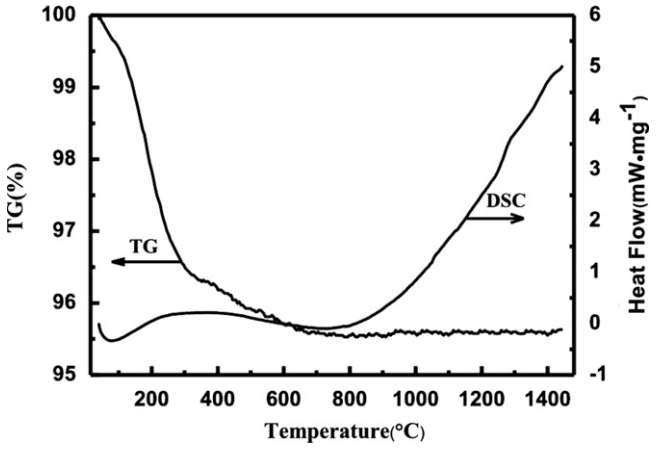

Fig. 3. DSC–TG curves of quartz glass fibers.

Table 1
Chemical composition of raw quartz glass fibers.

Analyte	SiO_2	Al_2O_3	Fe_2O_3	Na_2O	TiO_2	CaO	MoO_3	K_2O
Result (wt%)	98.29	1.01	0.29	0.18	0.13	0.06	0.02	0.02

the increase of heat treatment temperature, which indicates that the crystallization reaction of α-cristobalite is mostly completed and all the crystallization phase is α-cristobalite at 1435 °C. Because of the smaller diameter (~7.5 μm) and larger surface energy, quartz glass fibers have distinct difference with quartz glass, and the crystalline properties of quartz glass fibers are easily influenced by atmosphere, impurities and adsorbed element. The nucleation process first occurs at the surface of quartz fibers, and then the interior homogenous nucleus formation is driven by the surface nucleation. With further increase in heat treatment temperature to 1450 °C, quartz fibers and α-cristobalite commence melting and the intensity of the diffraction peak is slightly weakened, which is ascribed to the damaged integrality of partial α-cristobalite crystals (Fig. 5(i)). Fig. 5 displays the microstructure evolution of the quartz fibers heat-treated at 985–1450 °C. As can be seen from Fig. 5(a), the surface of the original quartz fibers is smooth and integrated with favorable toughness. Furthermore, it can be seen that the original integrality of quartz fibers was gradually destroyed with the increase in heat treatment temperature. As for Fig. 5(d)–(f), the quartz fibers were prone to brittleness and fragility along with the increase of crystallizing α-cristobalite phase from quartz glass fibers. The transformation process from quartz glass phase to α-cristobalite crystalline state is comprised of the reordering of silicon and oxygen atoms, the altering of Si–O covalent bond angles and the rearranging of space structure. Additionally, it is well demonstrated that the external bumped defective structure of quartz fibers was gradually stripped and chalked (Fig. 5(g) and (h)), which accounts for the disabled heat shield function of quartz glass fiber fabrics exposed to high temperatures for a long time.

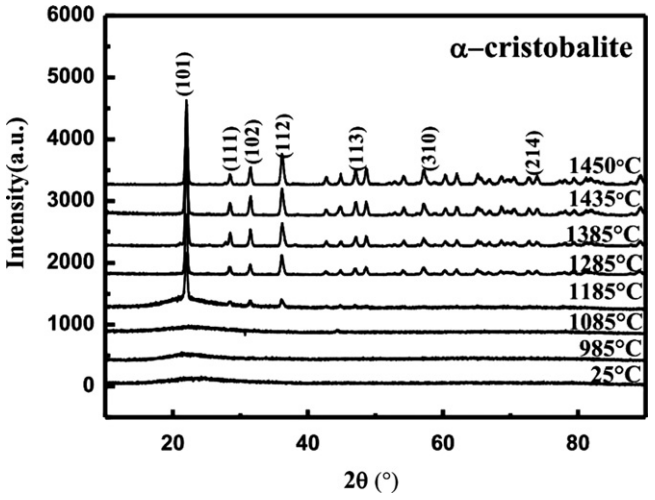

Fig. 4. XRD patterns of quartz glass fibers before and after heat treatment.

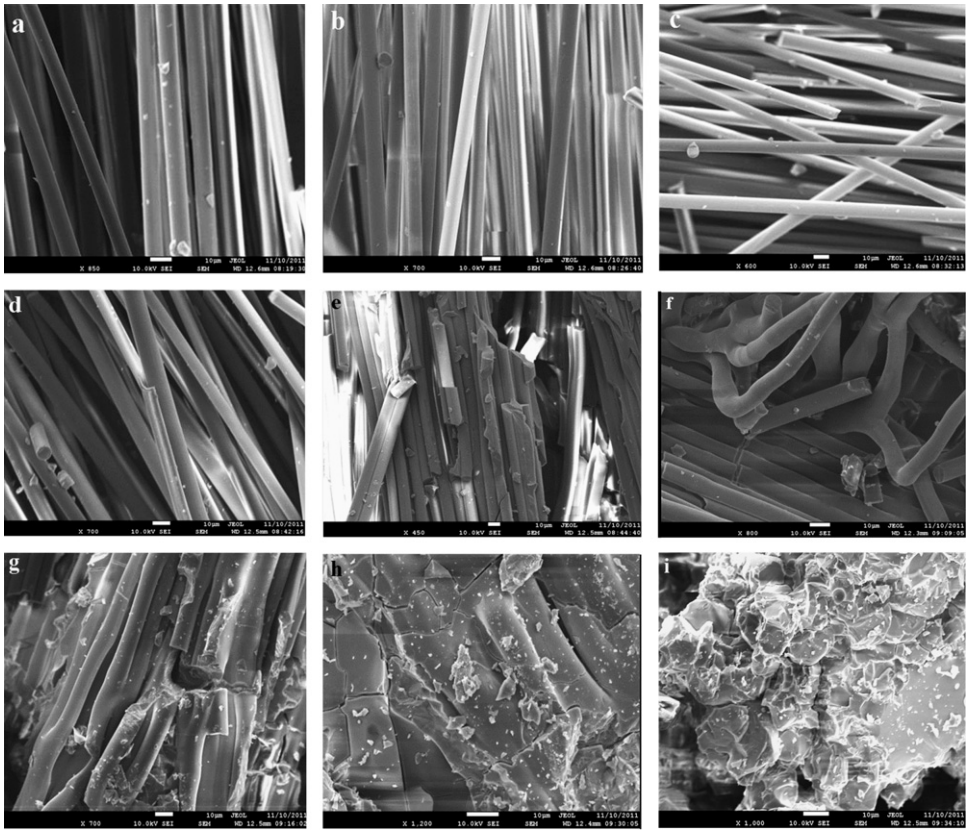

Fig. 5. Scanning electron microscope images of the quartz glass fibers heat-treated at different temperatures for 2 h: (a) 25 °C, (b) 985 °C, (c) 1085 °C, (d) 1185 °C, (e) 1285 °C, (f) 1385 °C, (g) 1410 °C, (h) 1435 °C and (i) 1450 °C.

3.2. Characterization of alumina–silica coatings

Fig. 6 shows the size distribution of different particles in incorporated α-alumina samples. Two kinds of high-purity (> 99.9%) α-alumina powders (S1 and S2) were initially dispersed in deionized water using ultrasonication to break down 'soft' agglomerates and for pH adjustment (to ~4) to provide a sufficient electrostatic repulsive force between particles to prevent flocculation. Fig. 6(a) with a broad and typically bimodal size distribution shows that the median Stokes diameter of S1 is ~16.24 μm. The plots of Fig. 6(b) indicate the median Stokes diameter of S2 is ~0.509 μm with a narrow and trimodal size distribution.

Fig. 7(a) shows the viscosity of the alumina–silica sol, as a function of shear rate. The plot shows a decrease in viscosity as the shear rate increases when the shear rate is lower than 0.27 s^{-1}. The alumina–silica sol shows a shear-thinning and non-Newtonian pseudoplastic behavior. When the shear rate is higher than 0.27 s^{-1} alumina–silica sol indicates a rheopectic behavior, which is not beneficial to the coating process. Fig. 7(b) shows the viscosity of the slurry of alumina–silica sol incorporated α-alumina, a shear-thinning and thixotropic behavior, which is beneficial to the coating process. As we can see from Fig. 7(b), the higher viscosity of S2 was recorded compared with the viscosity of S1 when the shear rate was increased. The higher-viscosity slurry is helpful to produce a thicker coating on the quartz fiber substrate, and thus the woven quartz fiber fabrics are porous and exhibit a strong adhesion to the alumina–silica sol incorporated α-alumina slurry.

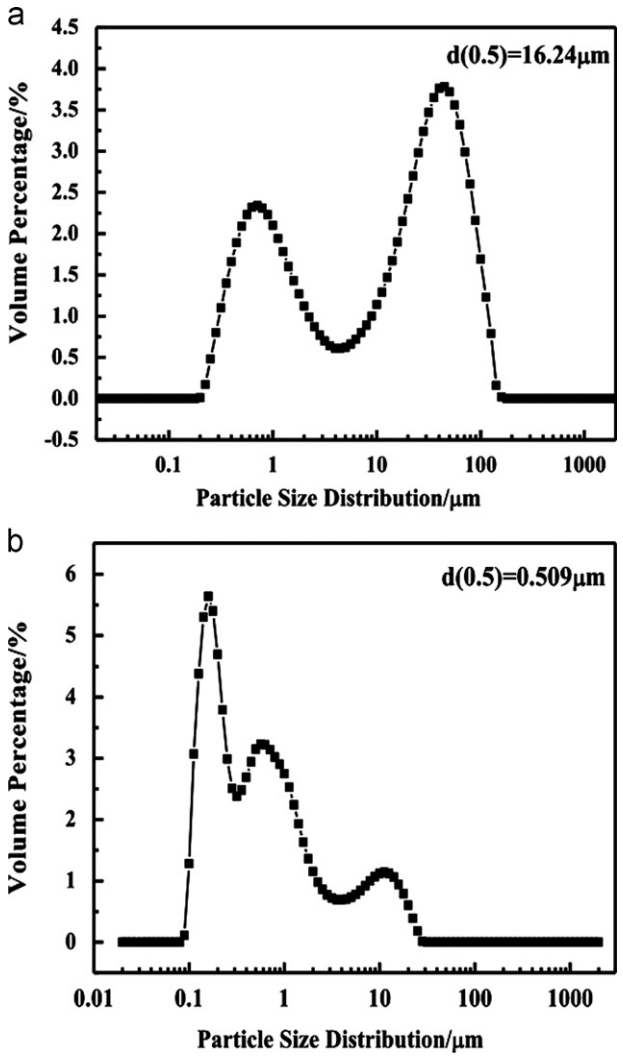

Fig. 6. Particle size distribution curves of incorporated α-alumina powders, S1 (a) and S2 (b).

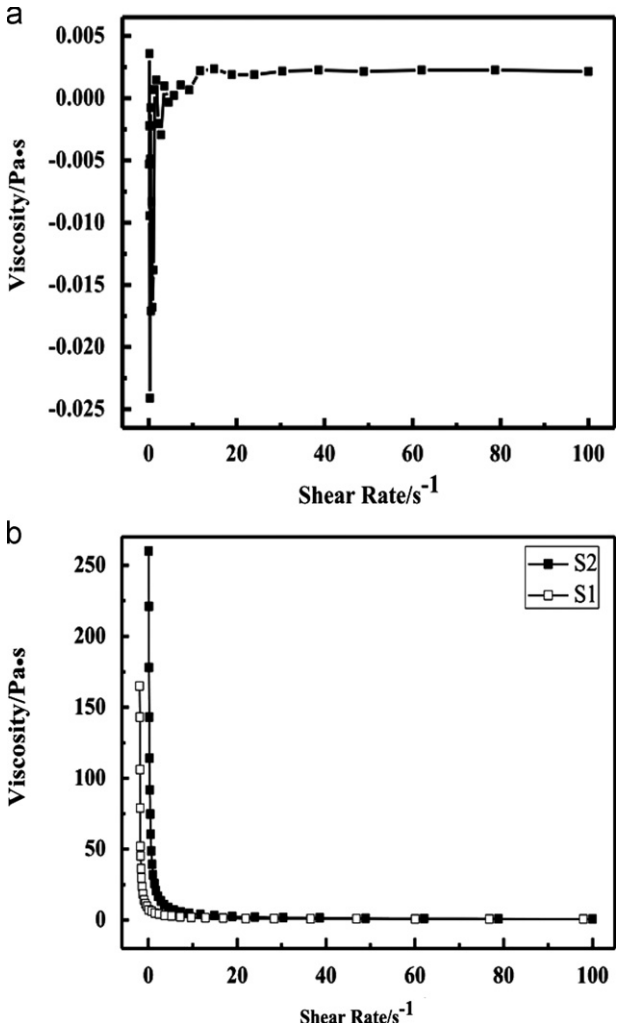

Fig. 7. (a) Viscosity of alumina–silica sol used to coat the quartz fiber substrate, as a function of shear rate and (b) viscosity of the slurry of alumina–silica sol incorporated α-alumina used to coat the quartz fiber substrate, as a function of shear rate.

SEM images of the alumina–silica sol incorporated α-alumina slurry (two dip-coating cycles) coatings on woven quartz fiber fabrics are represented in Fig. 8(a)–(c). On separate filaments a distinctive feature of this coating is smoothness and uniformity along the whole length and diameter of the fiber filament (Fig. 8(c)). As a whole, it is shown that the integrity, uniformity and smoothness of coatings are greatly affected by the particle size distribution

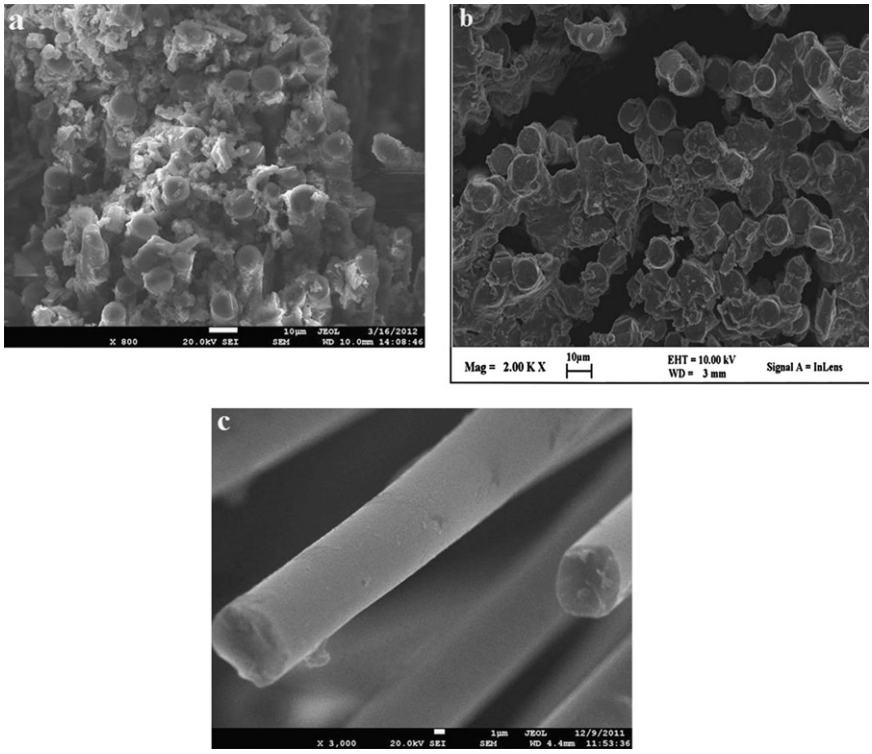

Fig. 8. Scanning electron microscope images of coated fibers with different incorporated α-alumina powders, heated at 950 °C for 2 h. (a): Incorporated S1α-alumina powder, (b) and (c) incorporated S2 α-alumina powder.

of initial incorporated α-alumina. Compared with Fig. 8(a), no de-bonding of coating on quartz fibers was observed, and the coverage of the quartz fibers was very uniform on a macroscopic scale in Fig. 8(b). The reason for the absence of de-bonding under thermal stresses could be the smaller particle size and well graded distribution of the S2 powder that allows crystals of coating to expand. However, the coverage was not complete, with discrete islands of particles developing rather than monolayer coverage, as shown in Fig. 8(a). The smaller particle size gave more uniform coverage with fewer agglomerates on the surface (Fig. 8(a) and (c)).

The SEM imaging and EDS microanalysis mapping performed on a cross-section of a coated and sintered ceramic coating indicated that the coatings consist of a homogeneous support that contains Si, O and Al. The element distribution of Si, O and Al throughout the whole SEM image was well-distributed, as shown in Fig. 9(b)–(d).The elemental microanalysis by SEM/EDS of alumina–silica/α-Al_2O_3 coated fibers taken from different areas indicates the presence of Si, O, and Al (Fig. 10). Since Si and O is present throughout the alumina/silica coatings as well as in the quartz fibers matrix, and Al is just present in the coatings, the counts of aluminum were smaller than that of silicon and oxygen in the quantitative analysis of the EDS curve.

Previous studies have shown that higher fracture toughness of α-alumina can be suitably combined with the lower thermal expand coefficient and higher creep resistance afforded by mullite. Mechanical tensile tests of original quartz fibers and coated quartz fibers were conducted by an Instron 1343 low-frequency fatigue tensile machine at room temperature, and the load was applied at a constant crosshead speed of 0.5 mm/min. About 5900 data for each type of fibers were tested. Because the tensile strength of quartz fibers can be greatly influenced by coating, it is very important to determine the tensile properties of the coated quartz fibers in order to evaluate the reinforcement ability of alumina–silica/α-Al_2O_3-coating for woven quartz fiber fabrics. Fiber tensile test results indicated that the tensile strength of quartz fibers with alumina–silica/α-Al_2O_3coatings was about 3.7 times that of the original quartz fibers (Fig. 11). The mechanical properties of coated fibers depend not only on mechanical properties of the raw fibers but also on the interfacial stress transfer capacity. The alumina–silica sol is used as a binder to provide a very high adhesive strength after the coating is successfully deposited on the woven quartz fiber fabrics, and the alumina–silica/α-Al_2O_3 coatings would provide compressive stress on quartz fibers, which would be beneficial to restrain and enhance the original fibers. The alumina–silica/α-Al_2O_3 coatings are not used for their load bearing contributions. As a result, when the alumina–silica/α-Al_2O_3 coated structure is subjected to loads, cracks typically develop within the coating before the substrate fails. Coating cracks usually initiate and rapidly propagate throughout the entire thickness of the coating. When the crack reaches the coating/substrate interface, the possibilities of alternative

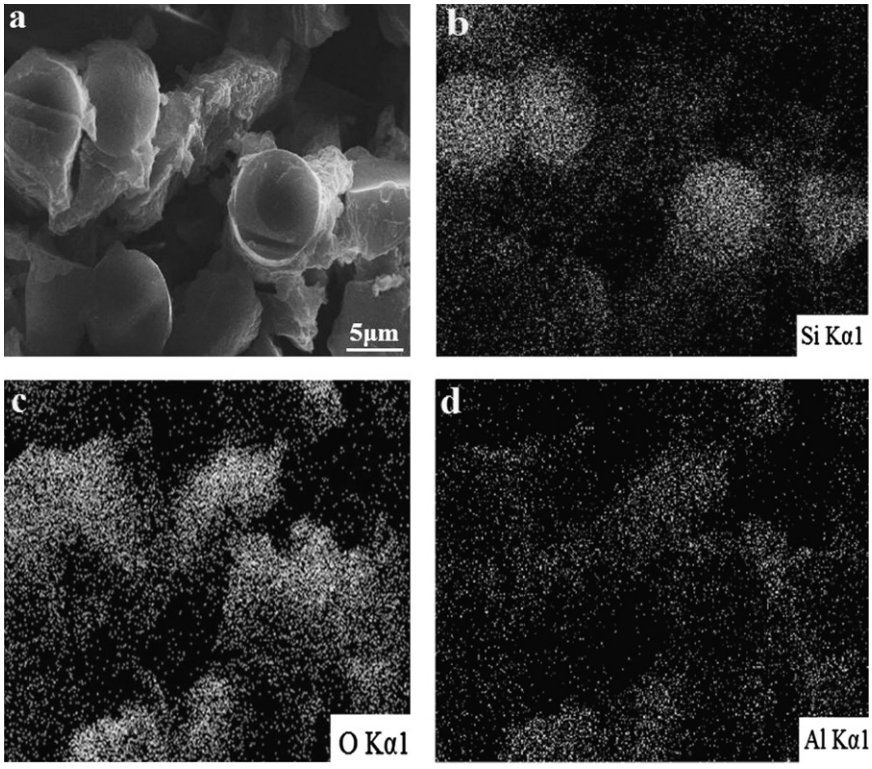

Fig. 9. SEM/EDS analysis of the alumina/silica-coated quartz fibers. (a) Scanning electron microscope image of coated fibers with incorporated S2 α-alumina powder, heated at 950 °C for 2 h; surface element distributions of Si (b), O (c) and Al (d) elements at the whole SEM image respectively.

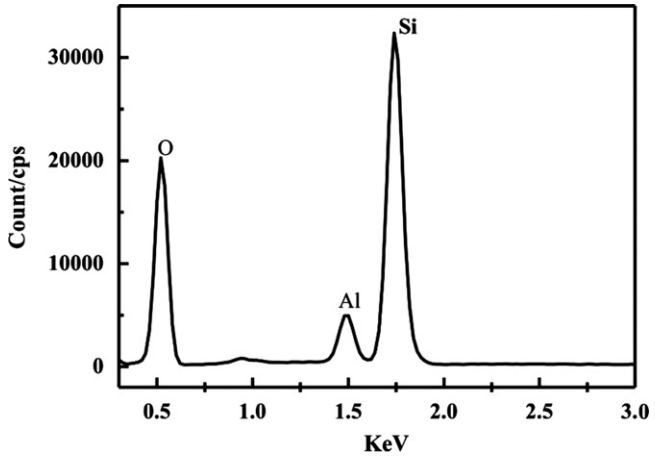

Fig. 10. EDS analysis data on cross section of the quartz fibers.

failure modes are surface embrittlement, where the crack enters the substrate causing quartz fiber failure, alumina–silica/α-Al_2O_3 coating delamination, where the crack turns and runs along the alumina–silica/α-Al_2O_3/quartz fibers interface, and multiple cracking, where the crack arrests but new cracks may form elsewhere after additional loading. The bonding strength between the alumina–silica/α-Al_2O_3 coating and quartz fibers is stronger than that among quartz fibers, therefore the extraction phenomenon of quartz fasciculi would occur with the cracking process. The yield point elongation indicates that the alumina–silica/α-Al_2O_3 coating can enhance the tensile strength as well as toughness, which is attributed to energy consumption of the quartz fibers pullout from alumina–silica/α-Al_2O_3 surroundings around the coating (Fig. 12).

The TEM images in Fig. 13 show the surface parts of alumina–silica/α-Al_2O_3-coated quartz fibers sintered at 1150 °C for 4 h. It can be seen from Fig. 13(b) that the sintered quartz fibers as a whole are still amorphous, and most of the regions are disordered. However, a small number of ordered nanometer areas, which exist in scattered distribution (Fig. 13(b)) correspond to selected-area electron diffraction (SAED) of alumina–silica/α-Al_2O_3-coated quartz fibers sintered at 1150 °C for 4 h. The image reveals diffuse scattering halos with few diffraction spots, which is due to the slight devitrification of cristobalite from quartz fibers. In order to further study the effect of alumina–silica/α-Al_2O_3 coatings on quartz fiber phase transformations, XRD spectrography is employed in this study, as is shown in Fig. 14. There is no obvious crystallization peak in the XRD pattern for the alumina–silica/α-Al_2O_3-coated quartz fibers sintered at 1150 °C for 4 h. However, compared with original quartz fibers the strength of the peak at around $2\theta = 22.15°$ (related with the α-cristobalite (101) crystal plane) becomes much stronger. The XRD image indicates that crystallization mainly occurs on quartz fiber surfaces, and the amount of α-cristobalite crystallites is quite small. Since alumina–silica/α-Al_2O_3 as the thermal barrier coating could protect quartz fibers from serious brittleness and degradation, it can be seen from Fig. 15(a) that the

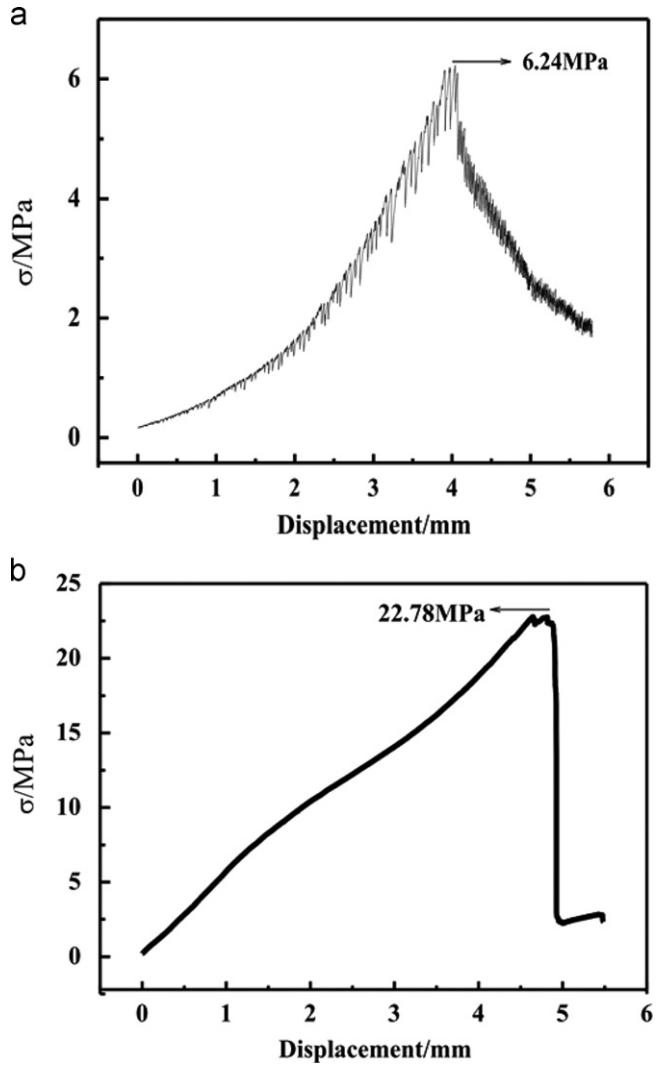

Fig. 11. Tensile strength–displacement curves of the original quartz fibers (a) and the coated alumina–silica/α-Al_2O_3 quartz fibers (b).

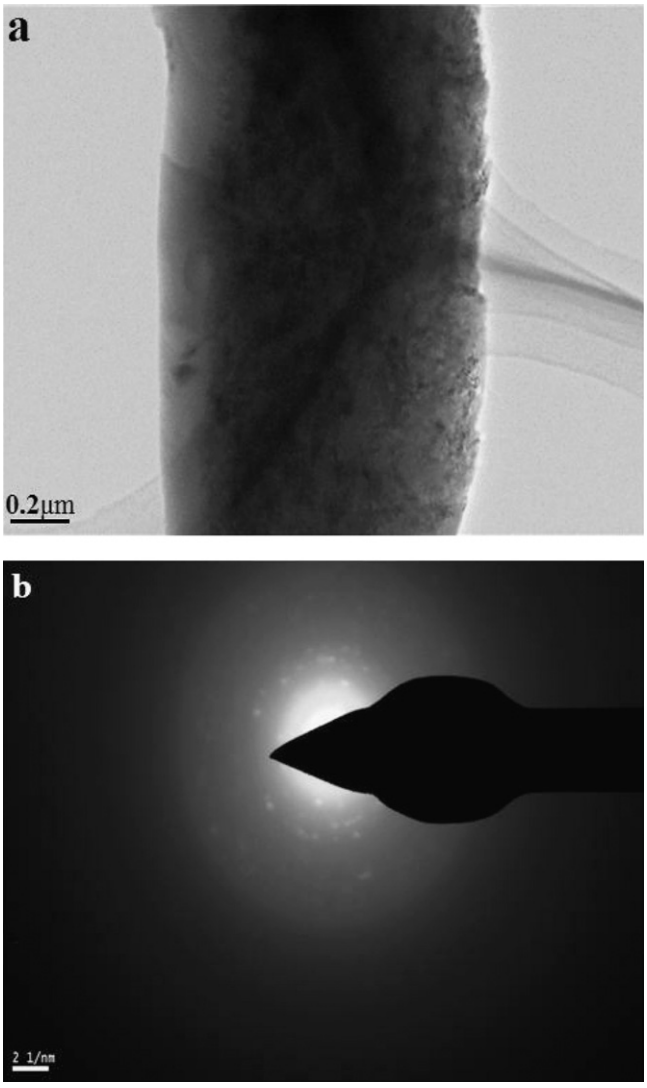

Fig. 13. TEM images of the surface part of alumina–silica/α-Al_2O_3 coated quartz fiber sintered at 1150 °C for 4 h (a), and (b) selected-area electron diffraction (SAED) pattern of alumina–silica/α-Al_2O_3 coated quartz fiber.

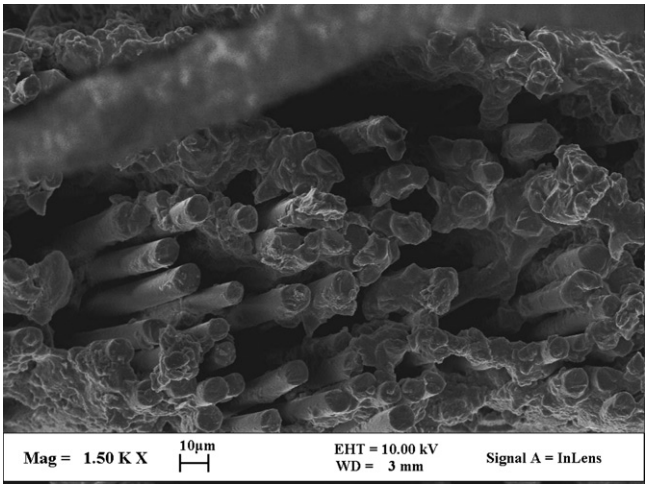

Fig. 12. Pullout surroundings around quartz fibers from the alumina–silica/α-Al_2O_3 coating.

alumina–silica/α-Al_2O_3-coated quartz fibers which sintered at 1150 °C for 4 h were without cracking and de-bonding. On the contrary, the brittle cracking and devitrification of original quartz fibers without coating sintered at 1150 °C for 4 h are observed in Figs. 14 and 15(b). It is considered that crystallization would cause the mismatch between α-cristobalite crystallized regions and amorphous quartz fibers and then present new defects and brittle cracking on fiber surfaces. Therefore, the alumina–silica/α-Al_2O_3 coatings actually play an important role in providing compressive stress on quartz fibers for the improvement of tensile strength and fracture toughness as well as thermal barrier coatings (TBCs).

Thermal diffusivity, bulk density and heat capacity of coatings and as-received quartz fibers are listed in Table 2. In order to directly compare the thermal protection capability of the alumina–silica/α-Al_2O_3 coating architectures, the thermal conductivity, λ, was calculated. The

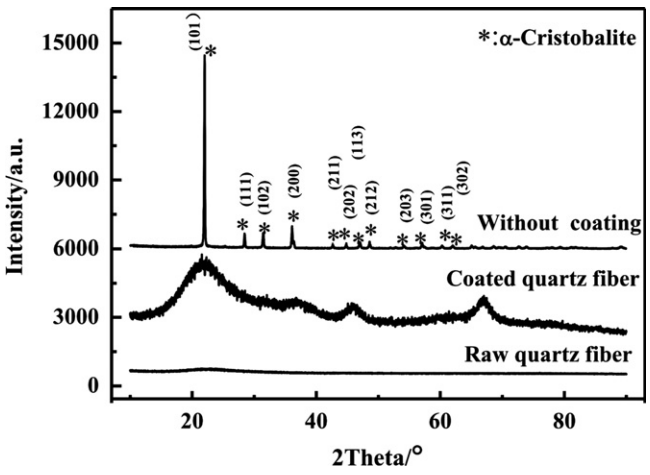

Fig. 14. XRD patterns of the as-received quartz fiber, quartz fiber with and without coating sintered at 1150 °C for 4 h.

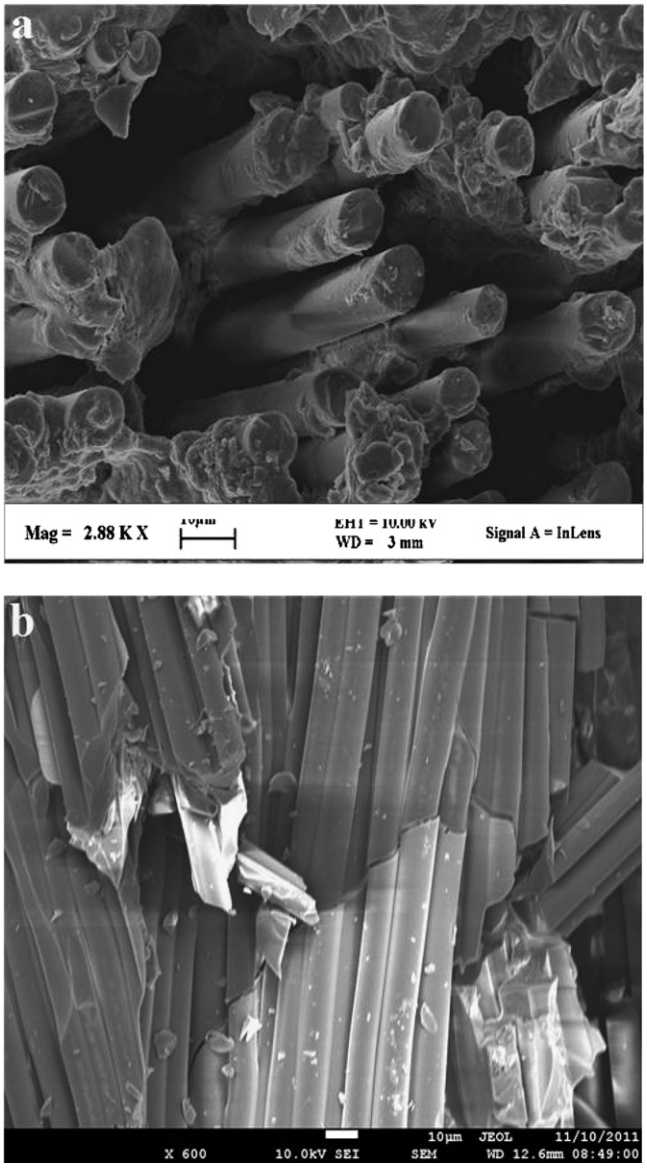

Fig. 15. Scanning electron microscope images of the quartz fibers with (a) and without (b) alumina–silica/α-Al_2O_3 coating, sintered at 1150 °C for 4 h.

corresponding thermal conductivity of the free-standing alumina–silica/α-Al_2O_3 coating and original quartz fibers are 1.27 W/m k and 1.87 W/m k respectively (298 K). Since mullite coatings [17–25] are particularly promising due to their high thermal stability, low thermal conductivity, high resistance to crack propagation and high thermal shock resistance, and previous studies have shown that the higher fracture toughness of α-alumina can be suitably combined with the lower thermal expand coefficient and higher creep resistance afforded by mullite. Therefore the alumina–silica/α-Al_2O_3 coating could lead to reduced thermal conductivity of coated quartz fiber composites by the modified sol–gel dip-coating technique with alumina–silica sol-incorporated coarse alumina powder as slurry. Compared with coated samples, it can be seen from Fig. 14 that the original quartz fibers without coatings through heat-treatment at 1150 °C for 4 h showed a crystalline structure, mostly composed of α-cristobalite, due to the devitrification from amorphous quartz, and the surface of that presents brittle cracking and degradation on fiber surfaces. Then the serious fiber brittleness, degradation and crystallization behavior become a severe limitation of quartz fibers as heat insulation and shielding function materials when exposed to high-temperature environments, especially above 1423 K. In this study, alumina–silica/α-Al_2O_3 coating are shown to be suitable for environmental protection of woven quartz fiber fabrics against thermal erosion in a high temperature environment.

4. Conclusion

Alumina–silica/α-Al_2O_3 coatings were deposited by a modified sol–gel dip-coating technique with alumina–silica sol-incorporated coarse alumina powder as slurry. Heat-treated original quartz fibers showed the initial crystallization temperature of α-cristobalite near 1100 °C, and the peak intensity of the α-cristobalite phase became stronger with the increase in thermal treatment temperature, which indicates that the crystallization reaction of α-cristobalite is mostly completed and all the crystallization phase is α-cristobalite at 1435 °C. Fiber tensile test results indicated that the tensile strength of quartz fibers with alumina–silica/α-Al_2O_3 coatings was about 3.7 times (22.78 MPa) that of the original quartz fibers. Compared with the original quartz fibers, the surface of the alumina–silica/α-Al_2O_3-coated quartz fibers sintered at 1150 °C for 4 h showed no cracking and de-bonding. TEM images showed that the coated quartz fibers after sintering at 1150 °C for 4 h were still amorphous and most of the regions were disordered, and the XRD images indicated no obvious crystallization peaks in the XRD pattern for the alumina–silica/α-Al_2O_3-coated quartz fibers sintered at 1150 °C for 4 h. The corresponding thermal conductivities of the free-standing alumina–silica/α-Al_2O_3 coating and original quartz fibers are 1.27 W/m k and 1.87 W/m k respectively (298 K). Alumina–silica/α-Al_2O_3 coatings actually play an important role in providing compressive stress on quartz

Table2
Thermal diffusivity, bulk density and heat capacity of coating and as-received quartz fibers.

Sample/parameters	Thermal diffusivity (mm^2/s)	Bulk density (g/cm^3)	Heat capacity ($J/g/^\circ C$)
Quartz fibers	1.08 ($T=298$ K)	2.19	0.79
Alumina–silica sol/Al_2O_3 coating	0.89 ($T=298$ K)	3.41	0.42

fibers for the improvement of tensile strength and fracture toughness as well as thermal barrier coatings (TBCs). In conclusion, crystallization would cause the mismatch between α-cristobalite crystallized regions and amorphous quartz fibers and then the surface of that presents brittle cracking and degradation. Then the serious fiber brittleness, degradation and crystallization behavior become a severe limitation of quartz fibers as heat insulation and shielding function materials when exposed to high-temperature environments. In this study, alumina–silica/α-Al_2O_3 coating are suitable for environmental protection of woven quartz fiber fabrics, against thermal erosion in a high temperature environment.

Acknowledgment

This work was financially supported by the National Natural Science Foundation of China (Nos. 11232008 and 51202117).

References

[1] N.I. Baklanova, T.M. Zima, A.I. Boronin, S.V. Kosheev, A.T. Titov, N.V. Isaeva, D.V. Graschenkov, S.S. Solntsev, Protective ceramic multilayer coatings for carbon fibers, Ceramics International 201 (2006) 2313–2319.
[2] Giovanni Di Girolamo, Caterina Blasi, Luciano Pilloni, Monica Schioppa, Microstructural and thermal properties of plasma sprayed mullite coatings, Ceramics International 36 (2010) 1389–1395.
[3] Yu Zheng, Shubin Wang, The effect of SiO_2-doped boron nitride multiple coatings on mechanical properties of quartz fibers, Applied Surface Science 258 (2012) 2901–2905.
[4] Changshu Xiang, Yubai Pan, Jingkun Guo, Electromagnetic interference shielding effectiveness of multiwalled carbon nanotube reinforced fused silica composites, Ceramics International 33 (2007) 1293–1297.
[5] Paul Heydt, Chongyang Luo, R. Clarke, Crystallographic texture and thermal conductivity of zirconia thermal barrier coatings deposited on different substrates, Journal of the American Ceramic Society 84 (2001) 1539–1544.
[6] Graziela Ávila Galhano, Luiz Felipe Valandro, Renata Marques De Melo, Roberto Scotti, Marco Antonio Bottino, Evaluation of the flexural strength of carbon fiber-, quartz fiber-, and glass fiber-based posts, Journal of Endodontics 31 (2005) 209–211.
[7] Satoshi Yamazaki, Kazuo Tsutsumi, Synthesis of an A-type zeolite membrane on silicon oxide film-silicon, quartz plate and quartz fiber filter, Microporous Materials 4 (1995) 205–212.
[8] P.W. Heitman, L.A. Shepard, T.H. Courtney, The effect of brittle interfacial compounds on deformation and fracture of molybdenum–aluminum fiber composites, Journal of the Mechanics and Physics of Solids 21 (1973) 75–89.
[9] H.V. Squires, H.W. Rayson, Thermal degradation of silica fibre-reinforced aluminium, Journal of Materials Science 12 (1977) 1010–1018.
[10] I. Al-Salim, A. Bagshaw, Antoine Bittar, Tim Kemmitt, A.James McQuillan, M. Mills, J. Ryan, Characterisation and activity of sol–gel-preparedTiO_2 photocatalysts modified with Ca, Sr or Ba ion additives, Journal of Materials Chemistry 10 (2000) 2358–2363.
[11] Yongjun Chen, D. Dionysiou, TiO_2 photocatalytic films on stainless steel: the role of Degussa P-25 in modified sol–gel methods, Applied Catalysis B: Environmental 62 (2006) 255–264.
[12] C. Jagadale, P. Takale, S. Sonawane, M. Joshi, I. Patil, B. Kale, B. Ogale, N-doped TiO_2 nanoparticle based visible light photocatalyst by modified peroxide sol–gel method, Journal of Physical Chemistry C 112 (2008) 14595–14602.
[13] Susan Trolier-McKinstry, Jiayu Chen, Kuppuswami Vedam, Robert E. Newnham, In situ annealing studies of sol–gel ferroelectric thin films by spectroscopic ellipsometry, Journal of the American Ceramic Society 78 (1995) 1907–1913.
[14] N. Barati, M.A. Faghihi Sani, H. Ghasemi, Preparation of uniform TiO_2 nanostructure film on 316L stainless steel by sol–gel dip coating, Applied Surface Science 255 (2009) 8328–8333.
[15] Sam Siau, Alfons Vervaet, Siska Degrande, Etienne Schacht, Andre Van Calster, Dip coating of dielectric and solder mask epoxy polymer layers for build-up purposes, Applied Surface Science 245 (2005) 353–368.
[16] A. Flores Renteria, B. Saruhan, U. Schulz, H.-J. Raetzer-Scheibe, J. Haug, A. Wiedenmann, Effect of morphology on thermal conductivity of EB-PVD PYSZ TBCs, Surface and Coatings Technology 201 (2006) 2611–2620.
[17] N. Lee, A. Miller, S. Jacobson, New generation of plasma-sprayed mullite coatings on silicon carbide, Journal of the American Ceramic Society 78 (1995) 705–710.
[18] Huang Jian-Feng, Zeng Xie-Rong, Li He-Jun, Xiong Xin-Bo, Huang Min, Mullite-Al_2O_3–SiC oxidation protective coating for carbon/carbon composites, Carbon 41 (2003) 2825–2829.
[19] Rao P. Mulpuri, Vinod K. Sarin, Synthesis of mullite coatings by chemical vapor deposition, Journal of Materials Research 11 (1996) 1315–1324.
[20] J.Allen Haynes, J. Lance, M. Cooley, K. Ferber, A. Lowden, P. Stinton, C.V.D. Mullite, Coatings in high-temperature, high-pressure air–H_2O, Journal of the American Ceramic Society 83 (2000) 657–659.
[21] P.S. Kisly, V.Yu. Kodash, The mullite coatings on heaters made of molybdenum disilicide, Ceramics International 15 (1989) 189–191.
[22] N. Lee, A. Miller, Development and environmental durability of mullite and mullite/YSZ dual layer coatings for SiC and Si_3N_4 ceramics, Surface and Coatings Technology 86–87 (1996) 142–148.
[23] S. Jacobson, J. Opila, N. Lee, Oxidation and corrosion of ceramics and ceramic matrix composites, Current Opinion in Solid State and Materials Science 5 (2001) 301–309.
[24] H. Rüscher, Holger Fritze, Günter Borchardt, Thomas Witke, Bernd Schultric, Mullite coatings on SiC and C/C–Si–SiC substrates characterized by infrared spectroscopy, Journal of the American Ceramic Society 80 (1997) 3225–3228.
[25] Mohamed Atik, Pedro De Lima Neto, A. Avaca, A. Aegerter, Sol–gel thin films for corrosion protection, Ceramics International 21 (1995) 403–406.